UNIFYING MANOEUVRE AND GUST LOADS ANALYSIS MODELS

Thiemo M. Kier[1] and Gertjan H. N. Looye[2]

[1]German Aerospace Center
DLR-Oberpfaffenhofen
Institute of Robotics and Mechatronics
82234 Wessling, GERMANY
Thiemo.Kier@dlr.de

[2]Gertjan.Looye@dlr.de

Keywords. Flight Loads Analysis, Gust Loads, Manoeuvre Loads, Flight Mechanics, Integrated Model.

Abstract. This paper proposes an approach for developing integrated aircraft flight loads models that may be used for used for both manoeuvre as well as gust loads analysis. These types of analysis are traditionally based on models of very different nature. Models for manoeuvre loads analysis are based on nonlinear rigid body equations of motion to account for large amplitude responses as resulting from prescribed, aggressive pilot inputs. Airframe flexibility is accounted for only quasi-statically by correction factors in the aerodynamic database. Models for gust loads analysis on the other hand, only consider small perturbations around a trimmed flight state. In this case, both structural dynamics as well as unsteady aerodynamic effects are important. Linear equations of motion are simulated in the frequency domain, since unsteady aerodynamic methods such as the Doublet Lattice Method (DLM) are readily available for this purpose.

The use of separate models for gust and manoeuvre loads analysis has important drawbacks. For example, it not possible to study the combined effect of extreme manoeuvres and gusts. Structural dynamic effects may induce additional loads, which are currently not accounted for in manoeuvre loads analysis. Furthermore, flight control systems (FCSs) contain many nonlinearities, requiring considerable effort to address these in linear frequency domain simulations.

This paper develops practical methods for development of integrated flight loads models. This is achieved by using a suitable set of fully flexible equations of motion, coupled with nonlinear quasi-steady aerodynamics and linear unsteady aerodynamics. The quasi-steady aerodynamic model accounts for more involved flight mechanical effects such as yaw-rolling coupling and induced drag. These nonlinear effects are modelled by using classical Vortex Lattice Method Aerodynamic Influence Coeffcients (AIC) with refined boundary conditions, but also higher fidelity methods may be used if available. Unsteady Aerodynamics are accounted for by an Rational Function Approximation (RFA) of the DLM matrices according to Roger's method. As an important contribution, this paper explains how to set up the RFA and how to define boundary conditions, such that quasi-steady and unsteady aerodynamic effects are appropriately separated. This approach makes the integration with nonlinear quasi-flexible aerodynamic databases considerably simpler and also allows the effect of gust penetration to be modelled more efficiently for use in the time domain. As a validation example, comparisons between a classical frequency domain gust model and the new proposed modelling scheme are presented for discrete gust responses.

1 INTRODUCTION

For certification of an aircraft, it has to be demonstrated that its structure can withstand the loads acting on it without damage. In order to design the structure accordingly, a so called loads envelope has to be computed. This loads envelope is comprised of critical combinations of flight conditions, i.e. altitude, Mach number, mass configurations and excitations. These so called load cases are specified for commercial aircraft in the CS/FAR Part 25 Subpart C Regulations [1].

The inputs for loads analysis models are generally a Finite Element Model (FEM) containing the stiffness and mass data for each mass case, the steady and/or unsteady aerodynamic loading at the specified Mach number, control laws of the Flight Control System (FCS) influencing the control surface deflections, dependent on the current flight state, and information about the systems, such as actuator transfer functions. The model is then subjected to external disturbances, such as gusts, or excited by pilot inputs. In [2] an approach to standardize an efficient dynamic model integration process was presented.

Traditionally, manoeuvre and gust loads analyses are carried out using different types of models that accommodate the specific needs of the involved disciplines. Table 1, summarizes the strategies for setting up different analysis models for static manoeuvres, dynamic manoeuvres and gust load analysis. Static manoeuvre loads, such as e.g. the symmetric

	Equations of Motion	Aerodynamics
Static Man. Loads	linear elastic EoM using inertia relief.	quasi-steady linear VLM with corrected lift gradients
Dynamic Man. Loads	6-DOF rigid nonlinear EoM solved in time domain, as used in flight mechanical simulations.	quasi-steady aerodynamics with nonlinear effects, mainly due to α. Aeroelastic effects are usually addressed by a database populated with results from static manoeuvre calculations.
Gust Loads	generalized linear elastic EoM solved in frequency domain.	unsteady aerodynamics from a linear harmonic DLM

Table 1: Comparison of modelling strategies for different loads analyses models

2.5g pull-up, are typically calculated using linear elastic equations of motion (EoM), as implemented for instance in commercial packages like `NASTRAN` [3]. These EoM use inertia relief schemes to account for the mass effects of an free flying aircraft and can be used in a modally reduced form or on the physical structural grid. The aerodynamics are accounted for by a Vortex Lattice Method (VLM) coupled to the structure by a so called spline matrix.

Dynamic manoeuvre loads analyses involve large rigid body movements and aerodynamic nonlinearities, e.g. over an angle of attack range. Also, the nonlinear Flight Control System (FCS), including Load alleviation Functions (LAF) plays an important role. Therefore, nonlinear equations of motion, as used in flight mechanical simulations are employed. Typically, these simulations account for aeroelastic effects by using a "flexibilized" aero-

dynamic database, populated with results from static manoeuvre calculations. Unsteady aerodynamic effects only play a minor role and are usually neglected or modelled rather crudely.

Gust loads analysis models compute small perturbations around a trimmed flight state, using modally reduced linear elastic equations of motion. Subsequently, the loads of the trimmed flight state from a static manoeuvre load case have to be superimposed. Unsteady aerodynamic effects are essential to capture the accurate loads levels. These types of models are typically solved in the frequency domain, where linear unsteady aerodynamics are conveniently available through the Doublet Lattice Method (DLM) [4]. Methods to account for nonlinearities introduced by Flight Control Systems in these types of simulation have been presented in [5, 6].

Employing different types of loads analysis models always bears the risk of introducing inconsistencies, e.g. when input data with different status is used. An approach is proposed to unify gust and manoeuvre loads models for simulation in the time domain, by using a suitable set of fully flexible equations of motion that are able to capture large nonlinear motions. The quasi-steady aerodynamic model, based on the VLM is enhanced to account for more involved flight mechanical effects such as yaw-rolling coupling and induced drag, by refining the boundary conditions. Unsteady Aerodynamics are accounted for by an Rational Function Approximation (RFA) of the DLM matrices according to Roger's method. The RFA is set up to adequately separate quasi-steady from unsteady aerodynamic effects. Transformation of the rigid body aerodynamics, necessary for coupling with the nonlinear equations of motion will be discussed. Discrete gust excitation and how to avoid the problematic approximation of the gust column is also addressed by the proposed scheme. Finally, a validation for a discrete gust load case, comparing the proposed method with the classical frequency domain approach is presented.

2 EQUATIONS OF MOTION

When setting up the equations of motion for a loads analysis of a flexible aircraft, the finite element stiffness model needs to be reduced. The model reduction is done by employing a Guyan reduction [7], with condensation points along a loads reference axis. The mass distributions are prepared for the corresponding payload/fuel cases. Subsequently a modal analysis is carried out and only part of the modal basis is retained to reduce the computational cost.

2.1 Linear Equations of Motion

The modally reduced linear equations of motion expressed in the frequency domain and explicitly partitioned in a rigid body ($b-set$) and flexible part ($f-set$), are given as.

$$\left\{ -\omega^2 \begin{bmatrix} \mathbf{M}_{bb} & \mathbf{0} \\ \mathbf{0} & \mathbf{M}_{ff} \end{bmatrix} + i\omega \begin{bmatrix} \mathbf{0} & \mathbf{0} \\ \mathbf{0} & \mathbf{B}_{ff} \end{bmatrix} + \begin{bmatrix} \mathbf{0} & \mathbf{0} \\ \mathbf{0} & \mathbf{K}_{ff} \end{bmatrix} \right\} \begin{bmatrix} \mathbf{u}_b \\ \mathbf{u}_f \end{bmatrix} = \begin{bmatrix} \mathbf{\Phi}_{gb}^{\mathrm{T}} \\ \mathbf{\Phi}_{gf}^{\mathrm{T}} \end{bmatrix} \mathbf{P}_g^{ext}(\omega) \qquad (1)$$

This type of EoM only accounts for small perturbations and is the usual form used for gust load analysis. The external forces $\mathbf{P}_g^{ext}(\omega)$ on the structural grid ($g-set$) are dependent on the rigid body and flexible motion, as well as atmospheric disturbances from the discrete gust. The combined set of rigid and flexible part is called $h-set$, consequently, the modal matrix is then $\mathbf{\Phi}_{gh} = \begin{bmatrix} \mathbf{\Phi}_{gb} & \mathbf{\Phi}_{gf} \end{bmatrix}$.

2.2 Nonlinear Equations of Motion

Accounting for large motions similar to a flight mechanics analysis, is required for dynamic manoeuvres. A derivation of a set of equations of motion suitable for this purpose is given in [8–11]. The nonlinear equations of motion describe the movement relative to a "mean axes" body reference frame. Its orientation an d poition are defined by constraints, based opn minimum relative momentum and angular momentum of flexible deformation wrt these axes. These constraints are usually applied in linearized form (practical mean axes constraints), resulting in a so called Buckens frame [12]. A detailed discussion about different floating reference frames can be found in the paper by Canavin [13]. Advantageously, the free-free vibration modes of a normal modes analysis automatically fulfill the "pratical mean axes" constraints.

The simplifying assumptions made during the course of derivation of the unrestrained equations of motion of a flexible aircraft are:

1. an earth fixed inertial reference system is assumed, neglecting the earth rotation.
2. gravity is uniform within this reference system.
3. the structure is composed of lumped masses.
4. Hooke's law is valid, i.e. deformations are small.
5. Eigenvectors are available from a modal analysis and are orthogonal w.r.t. the mass matrix.
6. deformations and rate of deformations are small and co-linear, i.e. their cross product can be neglected.
7. the tensor of inertia is assumed constant.

The derivation, yields the following equations of motion for an unrestrained flexible aircraft:

$$\begin{aligned} \begin{bmatrix} \mathbf{m}_b \left(\dot{\mathbf{V}}_b + \boldsymbol{\Omega}_b \times \mathbf{V}_b - \mathbf{T}_{bE}\, \mathbf{g}_E \right) \\ \mathbf{J}_b \dot{\boldsymbol{\Omega}}_b + \boldsymbol{\Omega}_b \times (\mathbf{J}_b \boldsymbol{\Omega}_b) \end{bmatrix} &= \boldsymbol{\Phi}_{gb}^{\mathrm{T}} \mathbf{P}_g^{ext}(t) \\ \mathbf{M}_{ff} \ddot{\mathbf{u}}_f + \mathbf{B}_{ff} \dot{\mathbf{u}}_f + \mathbf{K}_{ff} \mathbf{u}_f &= \boldsymbol{\Phi}_{gf}^{\mathrm{T}} \mathbf{P}_g^{ext}(t) \end{aligned} \tag{2}$$

where $\boldsymbol{\Phi}_{gb}$ is the rigid body modal matrix about the center of gravity. $\mathbf{V}_b$ and $\boldsymbol{\Omega}_b$ are the velocity, respectively angular velocity in the body frame of reference. Matrix $\mathbf{T}_{bE}$ transforms the gravitational vector from an earth fixed E to the body fixed frame of reference b. In [11] a derivation without the last two assumption is carried out, preserving inertial coupling between the flexible and rigid body part.

2.3 Load recovery

In order to recover the nodal loads $\mathbf{P}_g$ acting on the structural grid, the force summation method (FSM) [14] is employed. The FSM requires the external forces to be available on the structural grid.

$$\mathbf{P}_g = \mathbf{P}_g^{ext} - \underbrace{\mathbf{M}_{gg} \left\{ \boldsymbol{\Phi}_{gb}\, \ddot{\mathbf{u}}_b \quad + \quad \boldsymbol{\Phi}_{gf}\, \ddot{\mathbf{u}}_f \right\}}_{\mathbf{P}_g^{iner}} \tag{3}$$

in the case of the nonlinear equations of motion (2), the rigid body acceleration is given as

$$\ddot{\mathbf{u}}_b = \begin{bmatrix} \dot{\mathbf{V}}_b + \boldsymbol{\Omega} \times \mathbf{V}_b - \mathbf{T}_{bE}\, \mathbf{g}_E \\ \dot{\boldsymbol{\Omega}}_b + \mathbf{J}_b^{-1} \left(\boldsymbol{\Omega}_b \times (\mathbf{J}_b \boldsymbol{\Omega}_b) \right) \end{bmatrix}. \tag{4}$$

Considerably simpler to employ is the so called Mode Displacement Method (MDM), where the internal loads are recovered using the physical stiffness matrix.

$$\mathbf{P}_g = \mathbf{K}_{gg}\mathbf{\Phi}_{gf}\ \mathbf{u}_f \tag{5}$$

The MDM uses a reduced modal basis for recovery of the entire internal loads, whereas for the FSM only the inertial loads are modally truncated. The FSM accounts for the static part directly on the physical grid, and therefore has a superior convergence behavior compared to the MDM. Additionally, the FSM allows to discern between the contributions of inertial and aerodynamic forces, which might be insightful for design decisions.

3 AERODYNAMIC THEORY

One of the key aspects of the loads analysis is the calculation of aerodynamic forces acting on the structure. A vast amount of theories is available, ranging from simple lifting line to high Fidelity Navier-Stokes CFD solvers. Despite advances in computer technologies, the large amount of load cases that have to be considered are still prohibitive for costly CFD calculations in the realm of loads loop calculations. Therefore, usually classical methods derived from potential theory, such as the Vortex Lattice Method (VLM) [15] are still in use.

3.1 Vortex Lattice Method

The Vortex Lattice Method (VLM) discretizes a lifting surface by trapeziodal shaped elementary wings, so called aerodynamic boxes. The aerodynamic lift is generated by placing a vortex along the quarter chord line of such an aerodynamic box. According to the Helmholtz theorems, such a vortex must either end at a solid surface, or extend to infinity. Hence, the bound vortex is extended at both corner points to infinity, forming the well known horseshoe shape with its legs pointing in free stream direction. The circulation strength $\mathbf{\Gamma}_j$ of the individual horseshoe vortices is then determined by the Biot-Savart-Law and meeting the flow compatibility condition, i.e. no perpendicular flow $\mathbf{v}_j$ through the solid surface at the control point at 3/4 chord, according to Pistolesi's theorem [16].

$$\mathbf{v}_j = \mathbf{A}_{jj}\mathbf{\Gamma}_j \tag{6}$$

Figure 1 depicts the geometry of an aerodynamic box. The load acting point is located at mid span, quarter chord ($l-set$) and the control point at three quarter ($j-set$) chord point, respectively. The box reference point ($k-set$) is at the center of the box. The panel chord is c_j and the span is b_j. The vector of the bound vortex is denoted by b_l.

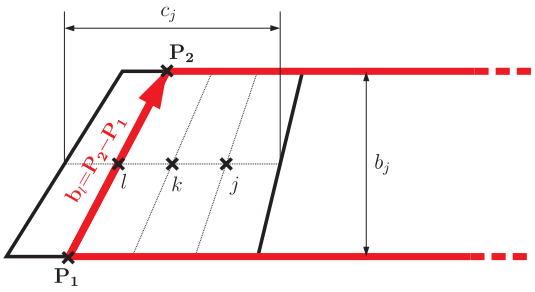

Figure 1: Geometrical properties of an aerodynamic box

To simplify the notation, all of the following equations are expressed for one aerodynamic box only. To extend the method for multiple boxes, all the derived matrices have to be expanded in a block-diagonal fashion.

The Kutta-Joukowsky-Law relates the circulation to the lifting force.

$$L_j = \rho U_\infty \Gamma_j b_j \tag{7}$$

Normalizing the velocities at the control point $\mathbf{w}_j = \frac{\mathbf{v}_j}{U_\infty}$ and inversion of (6), yields the differential pressure coefficients with the aerodynamic AIC matrix.

$$\Delta \mathbf{c}_{\mathbf{p}_j} = \mathbf{Q}_{jj} \mathbf{w}_j \tag{8}$$

Reversely, the circulation of an individual horseshoe vortex can be calculated from the pressure coefficient as follows.

$$\Gamma_j = U_\infty \frac{c_j}{2} \Delta c_{p_j} \tag{9}$$

This is the conventional implementation of the VLM as employed for instance in `NASTRAN`. Alternatively, the Kutta-Joukowsky-Law can be cast in the following form, involving a cross product instead of a scalar multiplication.

$$\mathbf{L}_l = \rho \mathbf{V}_l \times (\mathbf{b}_l \Gamma_j) \quad \text{with } \mathbf{L}_l, \mathbf{V}_l, \mathbf{b}_l \in \mathbb{R}^3 \text{ and } \Gamma_j \in \mathbb{R}^1 \tag{10}$$

The vector $\mathbf{b}_l$ is the vector quantity between the two corners of the horseshoe vortex, i.e. the bound vortex. The lift force $\mathbf{L}_l$ then acts, as aerodynamic theory predicts, perpendicular to the local stream velocity $\mathbf{V}_l$ at the quarter chord point. Equation (10) can be recast as

$$\mathbf{L}_l = q_\infty \Big(- c_j \ \mathbf{skew}(\mathbf{b}_l) \Big) \mathbf{w}_l \ \cdot \ \Delta c_{p_j} \, . \tag{11}$$

The vector $\mathbf{w}_l$ is the velocity at quarter chord normalized by the free stream velocity. The quantities with index l are elements in $\mathbb{R}^3$, whereas index j denotes elements in $\mathbb{R}^1$. Since $\mathbf{w}_l$ as well as $\mathbf{w}_j$ depend on the boundary conditions, the expression is inherently nonlinear and has to be multiplied on box level. Therefore, it is computationally more demanding compared to the linear expression. If $\mathbf{w}_l = \begin{bmatrix} 1 & 0 & 0 \end{bmatrix}^{\mathrm{T}}$, i.e. the free stream is exclusively in x-direction, the analysis simplifies to the conventional case, with the lift $\mathbf{L}_l$, acting in the z-direction only. Note that the y-component of $(\mathbf{b}_l)_y = \mathbf{b}_j$.

3.2 Induced drag

According to the Helmholtz theorems, the spanwise change of circulation of a 3D lifting surface leads to trailing vortices that are shed into the wake. The vorticity in the wake induces an additional downwash at the quarter chord of each box, which turn the lift vector rearwards. This rearward component is the so called induced drag. Following largely the derivation of Katz and Plotkin [17], the normalized induced velocity at the quarter chord is expressed as follows.

$$\mathbf{w}_{l_{ind}} = \mathbf{D}_{lj} \Delta c_{p_j} \tag{12}$$

The induced downwash matrix $\mathbf{D}_{lj}$ is equivalent to $\mathbf{A}_{jj}$ from (6) without the contributions from the bound vortex. The induced downwash then acts only in z-direction. To build up the effective stream direction $\mathbf{w}_l$, the induced component $\mathbf{w}_{l_{ind}}$ needs to be added to the

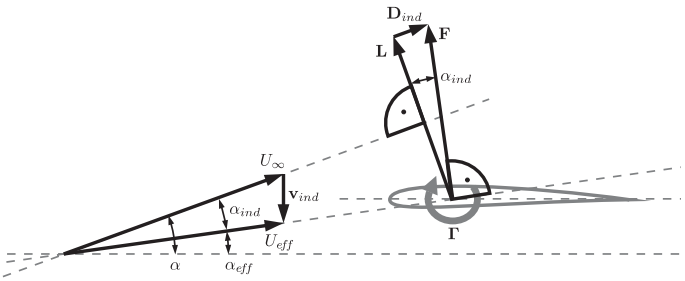

Figure 2: induced drag

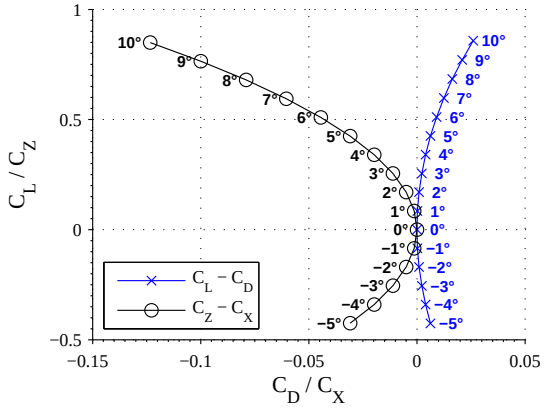

Figure 3: Drag polar in wind and in body axes

free stream and motion induced components, as illustrated in figure 2. Interesting to note is that despite the presence of an induced drag component, the force still acts forward in the body frame of reference, when neglecting friction and pressure drag components. Figure 3 illustrates the same drag polar in a wind and in a body axis coordinate system.

In figure 4 an example of a rectangular wing with aspect ratio $AR = 10$ is considered. The conventional method is contrasted to the proposed method including induced drag and lift forces acting perpendicular to the effective stream direction. For a simple angle of

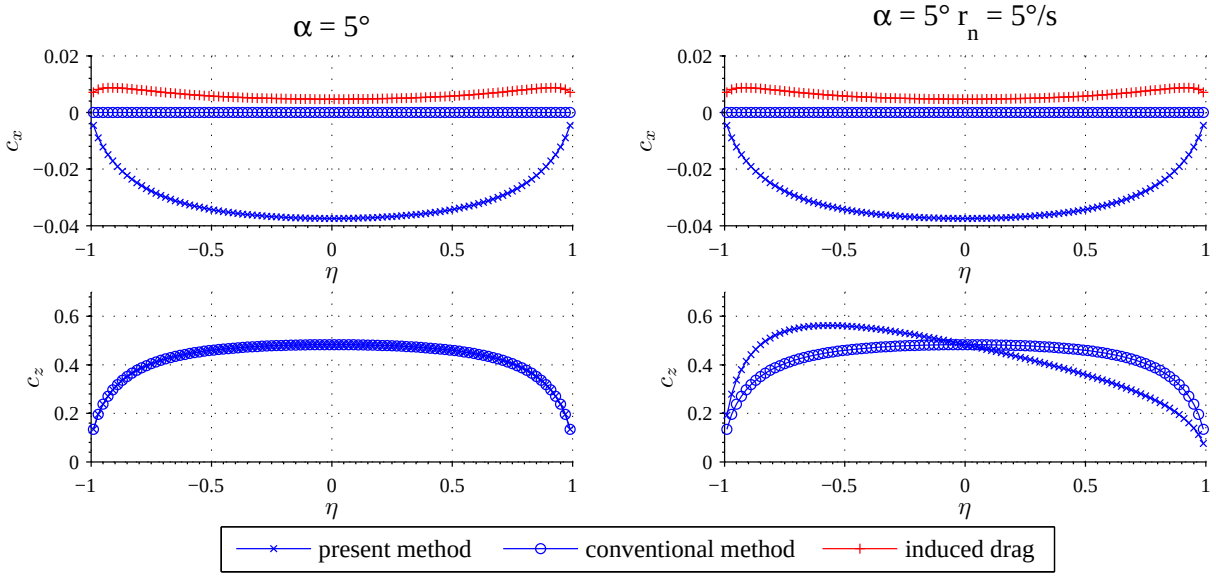

Figure 4: spanwise c_x and c_z distribution for present and conventional method

attack case, the lift acting in z-direction is identical for the conventional and present VLM. Additionally, the present method includes a component acting in in negative x-direction (forward). For better illustration, the component of the induced drag has been drawn separately. It can been seen that at areas of large spanwise lift gradients, the induced drag increases. At mid span, the induced drag is small and approaches zero, as the aspect ratio goes to infinity, in accordance with aerodynamic theory.

When considering a case with an additional yaw rate r_n, the present method shows a bias of the lift distribution. This can be attributed to the fact that the x-component of $\mathbf{w}_l$ is increased for the advancing wing, while it is decreased for the receding wing. This bias in the lift distribution induces a rolling moment. In contrast to the conventional method the present method is able to capture the yaw-roll coupling.

3.3 Doublet Lattice Method

So far only quasi-steady aerodynamics were considered. For gust loads analysis the unsteady aerodynamics are essential. The governing flow equation is the unsteady Prandtl-Glauert equation. The Doublet Lattice Method (DLM) provides a harmonic solution for this equation. Further, is uses the acceleration potential which is formally equivalent to the velocity potential equation. Therefore, the same elementary solutions are valid, e.g. the source potential. Analog to acoustics, the harmonically oscillating source is moved wrt a resting fluid, followed by a Gallilei transformation, which moves the observer with the source. Lift can not be generated by a source, hence the source potential is differentiated in the z-direction, yielding the doublet potential. The acceleration potential directly yields the pressure difference between the upper and lower surface, which makes additional steps, i.e. the use of the Kutta-Joukowsky Law, in the load recovery process unnecessary. However, the acceleration potential of the doublet still needs to be integrated to calculate the induced velocity, which is needed to meet the flow tangency condition on the lifting surface. Contrary to the velocity potential of a free flying wing, where there is a velocity jump across the wake surface, there is no such jump in the pressure, hence the wake needs not to be modelled.

The DLM [4] is the unsteady extension to the VLM, which similarly places the singularity along the quarter chord and satisfies the flow tangency at the three quarter chord. The doublet potential is evaluated at discrete points along the quarter chord line, which are used for a polynomial fit and its subsequent analytical integration. The integration still can not be performed in closed form and series approximations for parts of the kernel functions need to be employed. The final result for the pressure coefficient

$$\Delta\mathbf{c}_{\mathbf{p}_j}(k) = \mathbf{Q}_{jj}(k)\mathbf{w}_j(k) \tag{13}$$

has similar form to the conventional steady aerodynamics, where

$$k = \frac{c_{ref}/2}{U_\infty} \tag{14}$$

is is the reduced frequency. In fact, for $k = 0$ the DLM solution is replaced with the steady VLM results [18], since for this case no approximations are required.

4 AERODYNAMIC BOUNDARY CONDITIONS

This section explains how the boundary conditions for the VLM and DLM are obtained wrt the box reference point. The box center serves as reference point and is denoted

$k-set$, as depicted in figure 1. Depending on the displacement, respectively motion of the reference point, the normal velocity $\mathbf{w}_j$ at the control point and velocity at the quarter chord point $\mathbf{w}_l$ need to be determined. Further the lift acting on the $l-set$ point needs to be transferred back to the reference point as well.

In the conventional method the sets j,k, and l are introduced as follows.

$$\mathbf{u}_j = \begin{bmatrix} z \end{bmatrix}_j \; ; \; \mathbf{u}_k = \begin{bmatrix} z & \theta \end{bmatrix}_k^{\mathrm{T}} \; ; \; \mathbf{u}_l = \begin{bmatrix} z \end{bmatrix}_l \tag{15}$$

The $j-set$ contains only one Degree of Freedom (DoF) in z-direction, since, at the control point, only the normal velocity is of interest. For the conventional method, the lift is assumed to act only in z-direction at quarter chord. This induces a moment about the y-axis at the box reference point. Hence, the $k-set$ contains the two DoF z_k and θ_k. When the displacement of the reference point is considered, this corresponds to a box angle of attack.

For the present method the $l-set$ has to be extended to include all three translational degrees of freedom. When transferring the load from $l-set$ to $k-set$, moments in all directions are induced, therefore the $k-set$ needs to be extended to six degrees of freedom[1]. Hence, the displacement vectors $\mathbf{u}$ have the following degrees of freedom.

$$\mathbf{u}_j = \begin{bmatrix} z \end{bmatrix}_j \; ; \; \mathbf{u}_k = \begin{bmatrix} x & y & z & \varphi & \theta & \psi \end{bmatrix}_k^{\mathrm{T}} \; ; \; \mathbf{u}_l = \begin{bmatrix} x & y & z \end{bmatrix}_l^{\mathrm{T}} \tag{16}$$

The time derivatives of displacement vectors, normalized by the free-stream velocity are denoted by $\mathbf{w}$.

$$\mathbf{w}_j = \frac{\dot{\mathbf{u}}_j}{U_\infty} \; ; \; \mathbf{w}_l = \frac{\dot{\mathbf{u}}_l}{U_\infty} \tag{17}$$

These vectors, obeying the small angle assumption, correspond to local angles of attack. All of the associated matrices pertaining to the boundary conditions need to be extended with the additional degrees of freedom.

4.1 Differentiation matrices

The boundary conditions for the flow velocities at the quarter chord $\mathbf{w}_l$, respectively at the three quarter chord $\mathbf{w}_j$, need to be determined with respect to the panel reference point $\mathbf{u}_k$, by using so called differentiation matrices. The differentiation matrix $\mathbf{D^1}$ relates the steady displacement of the reference point $\mathbf{u}_k$ to the local velocities $\mathbf{w}_l$ and $\mathbf{w}_j$, while $\mathbf{D^2}$ does the same for the motion of the reference point $\dot{\mathbf{u}}_k$. Figure 5 illustrates how the differentiation matrices are determined.

The steady rotation θ_k directly translates to $\mathbf{w}_j$ at the control point. There are not further contributions, hence the matrix $\mathbf{D^1}_{jk}$ is formulated as follows.

$$\mathbf{w}_j = \underbrace{\begin{bmatrix} 0 & 0 & 0 & 0 & 1 & 0 \end{bmatrix}}_{\mathbf{D^1}_{jk}} \mathbf{u}_k \tag{18}$$

A normalized heaving motion $\dot{z}_k/U_\infty$ and a pitching motion $\dot{\theta}_k/U_\infty$ multiplied by the lever arm $-c_j/4$ lead to a $-\mathbf{w}_j$ contribution. The matrix $\mathbf{D^2}_{jk}$ is multiplied by $\frac{2}{c_{ref}}$, in order to

[1]Since both the $l-set$ and $k-set$ points are located in the same x-y plane, there is no need for the ψ component in the $k-set$, however for the sake of completeness it is introduced anyway.

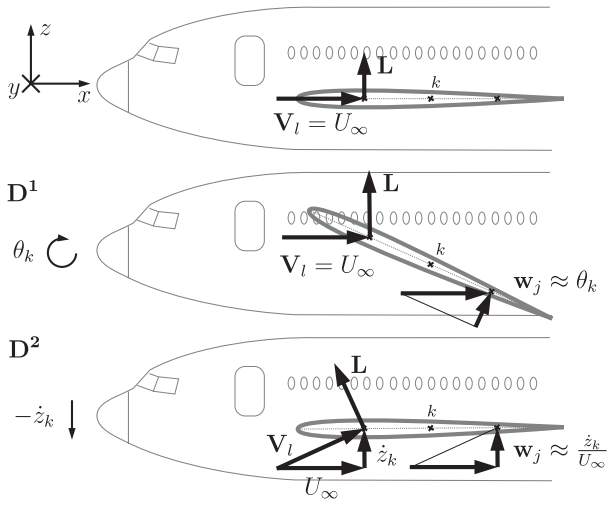

Figure 5: Explanation of the differentiation matrices $\mathbf{D^1}_{jk}$, $\mathbf{D^2}_{jk}$, and $\mathbf{D^2}_{lk}$

be compatible with the reduced frequency of eq. (14).

$$\mathbf{w}_j = \underbrace{-\tfrac{2}{c_{ref}} \begin{bmatrix} 0 & 0 & 1 & 0 & -c_j/4 & 0 \end{bmatrix}}_{\mathbf{D^2}_{jk}} \left(\tfrac{c_{ref}/2}{U_\infty}\right) \cdot \dot{\mathbf{u}}_k \tag{19}$$

$$\mathbf{w}_j = \mathbf{D^2}_{jk} \left(\tfrac{c_{ref}/2}{U_\infty}\right) \cdot \dot{\mathbf{u}}_k \tag{20}$$

Respectively, the matrix $\mathbf{D^2}_{lk}$ can be set up, for the three translational DoF at the quarter chord.

$$\mathbf{w}_l = \underbrace{-\tfrac{2}{c_{ref}} \begin{bmatrix} 1 & 0 & 0 & 0 & 0 & 0 \\ 0 & 1 & 0 & 0 & 0 & -c_j/4 \\ 0 & 0 & 1 & 0 & c_j/4 & 0 \end{bmatrix}}_{\mathbf{D^2}_{lk}} \left(\tfrac{c_{ref}/2}{U_\infty}\right) \cdot \dot{\mathbf{u}}_k \tag{21}$$

$$\mathbf{w}_l = \mathbf{D^2}_{lk} \left(\tfrac{c_{ref}/2}{U_\infty}\right) \cdot \dot{\mathbf{u}}_k \tag{22}$$

As can be seen by inspection, there is no matrix for $\mathbf{D^1}_{lk}$, as a steady deformation does not change the direction of flow. For the conventional VLM the two cases depicted in figure 5 lead to identical results, as the flow conditions at the control point are the same. For the present VLM, there is a significant difference between the two flow conditions, as the direction of the lift vector changes for the heaving motion, while remaining unchanged for the steady deflection case.

The flow conditions can then be expressed as a function of reduced frequency.

$$\mathbf{w}_j(k) = \left(\mathbf{D^1}_{jk} + ik\, \mathbf{D^2}_{jk}\right)\, \mathbf{u}_k \quad ; \quad \mathbf{w}_l(k) = ik\, \mathbf{D^2}_{lk}\, \mathbf{u}_k \tag{23}$$

4.2 Load transformation to panel mid point

With the flow conditions given, the lift vector can be calculated using the AIC matrices. Now the load at the box reference point needs to be determined. This is done by the matrix $\mathbf{T}_{lk}$ that transforms the load at the quarter chord point $l - set$ calculated by

equation (11) to the box mid point $k-set$. This replaces the conventionally used matrix $\mathbf{S}_{kj}$, which is used to transform directly the pressure coefficients to a load acting at box mid point. The index j is actually a misnomer, since the matrix $\mathbf{S}_{kj}$ assumes the load acting on the quarter chord, just like $\mathbf{T}_{lk}$. This is equivalent to setting $\mathbf{S}_{kj} = \mathbf{T}_{lk}^{\mathrm{T}} \cdot a_j$, where $a_j = c_j \cdot b_j$ is the box area.

4.3 Spline matrix

The aerodynamic properties are given with respect to the aerodynamic grid $k-set$. The matrix connecting the displacements of the the structural grid ($g-set$) to the aerodynamic grid ($k-set$) is called spline matrix $\mathbf{T}_{kg}$. For the present VLM, the $k-set$ had to be extended to six DoF, hence the spline matrix has to be extended to the full six $k-set$ DoF as well. The structural $g-set$ consists of all six DoF per grid point already.

The commonly used Infinite Plate Spline (IPS) [19] uses the radial basis function $\phi(r) = \|r\|^2 \ln(\|r\|)$, with $\|r_{kg}\| = \sqrt{(x_k - x_g)^2 + (y_k - y_g)^2}$. This radial basis function constitutes an analytical flat plate solution. All grid points (aerodynamic and structural) are transformed and projected onto the so called spline plane, which is defined by the lifting surface. The points are assumed to move with the deflection determined by the flat plate solution.

To extend the spline to six DoF, the solution for the deformation in z-direction is used for the x- and y-direction as well. These additional terms represent an in-plane deformation. Further, similar to the local angle of attack, which is obtained by differentiating the solution in chordwise, i.e. x-direction, the slope in spanwise direction can be calculated by differentiating in y-direction. For the IPS, the derivative wrt the z-direction is zero. The 6-DOF IPS spline matrix can be assembled as follows.

$$\mathbf{T}_{kg} = \left[\begin{array}{c|c} \mathbf{diag}\left(\begin{bmatrix}\mathbf{t}_{kg} & \mathbf{t}_{kg} & \mathbf{t}_{kg}\end{bmatrix}^{\mathrm{T}}\right) & \mathbf{0}_{3\times3} \\ \hline \mathbf{skew}\left(\begin{bmatrix}\frac{\partial \mathbf{t}_{kg}}{\partial x_k} & \frac{\partial \mathbf{t}_{kg}}{\partial y_k} & \frac{\partial \mathbf{t}_{kg}}{\partial z_k}\end{bmatrix}^{\mathrm{T}}\right) & \mathbf{0}_{3\times3} \end{array}\right] \tag{24}$$

Using the modal matrix for the flexible deformations $\mathbf{\Phi}_{gf}$, the deformation of the aerodynamic DoF can be related to the modal displacements from the equations of motion.

$$\mathbf{u}_k(k) = \mathbf{T}_{kg}\mathbf{\Phi}_{gf}\mathbf{u}_f(k) \tag{25}$$

4.4 Control surface modes

For loads analysis purposes, usually there are no control surface modes present in the modal basis $\mathbf{\Phi}_{gf}$, since they were not modelled as structural parts. The control surfaces can be included as rigid body rotations of the associated aerodynamic boxes about a hinge axis.

$$\mathbf{u}_k(k) = \mathbf{\Phi}_{kx}\mathbf{u}_x(k) \tag{26}$$

The control surface matrix $\mathbf{\Phi}_{kx}$ can be treated in the same way as the structural modes.

5 TIME DOMAIN UNSTEADY AERODYNAMICS

The main reason, that gust load calculations are done in the frequency domain, is the availability of tabulated unsteady aerodynamic matrices as function of reduced frequency through the DLM.

5.1 Rational Function Approximation

To make the frequency domain unsteady aerodynamics usable for time domain calculations provision need to be taken. One possibility is to fit the tabulated frequency data with rational functions. Consequently, this method is called Rational Function Approximations (RFA). This form can be expressed in the Laplace domain and thus be used for time domain simulations. For a shorter notation, it is convenient to introduce an equivalent to the reduced frequency k in the Laplace domain denoted by s^*.

$$ik = i\omega \left(\frac{c_{ref}/2}{U_\infty}\right) \Leftrightarrow s^* = s \left(\frac{c_{ref}/2}{U_\infty}\right) \tag{27}$$

The RFA captures the time dependent behavior of the unsteady flow by introducing of additional aerodynamic states, so called lag states. Many flavors of this method have been published [20–23], with improvements leading to systems with fewer lag states.

Most publications concentrate on approximation of the generalized aerodynamic matrices $\mathbf{Q}_{hh}$, i.e. the AIC matrices are already multiplied with the differentiation matrices (23) and the modal basis. This approach has three significant disadvantages. Firstly, the aerodynamic forces are not available on the structural grid, making the use of the FSM (3) impossible, although this can be fixed by approximation of the half generalized aerodynamic matrices $\mathbf{Q}_{gh}$. Secondly, and more importantly, the steady and unsteady contributions can not be discerned anymore. And thirdly, the approximation becomes tied to a mass case, whereas a physical approximation is only dependent on the Mach number.

Here, a scheme is proposed to approximate directly the physical AIC matrices $\mathbf{Q}_{jj}(k)$, using Roger's method [20].

$$\mathbf{Q}_{jj}(s^*) = \mathbf{Q^0}_{jj} + \mathbf{Q^1}_{jj} s^* + \sum_{i=1}^{n_p} \mathbf{Q^{L}}_{i\,jj} \frac{s^* \mathbf{I}}{s^* + p_i} \tag{28}$$

The term $\mathbf{Q^0}_{jj}$ represents the quasi-steady term, $\mathbf{Q^1}_{jj}$ is the added mass, and the $\mathbf{Q^{L}}_{i\,jj}$ with the predefined poles p_i terms are responsible for the lagging behavior of the unsteady flow. Interesting to note is the absence of the $\mathbf{Q^2}_{jj}$ acceleration term in the physical approximation. Notably, in the original paper of Roger [20], the approximation was also done prior to multiplication with the differentiation matrices, however no added mass term was considered. The relation between the approximation of the physical AICs without the acceleration term and the approximation of the generalized AIC matrices with an acceleration term is explained in the appendix in section 8.

5.2 Realization of the system

The system (28) can be now used for the time domain simulation. Pre-multiplying equation (28) with $\mathbf{T}_{kg}^{\mathrm{T}} \mathbf{S}_{kj}$, the approximation can be expressed as a left hand side realization.

$$\begin{aligned}\mathbf{Q}_{gj}(s^*) = {} & \mathbf{Q^0}_{gj} + \mathbf{Q^1}_{gj} s^* + \\ & \underbrace{\begin{bmatrix}\mathbf{Q^{L}}_{1\,gj} & \dots & \mathbf{Q^{L}}_{n_p\,gj}\end{bmatrix}}_{\mathbf{D}} \left(s^* \mathbf{I} - \underbrace{\mathbf{diag}\left(\begin{bmatrix}-p_1\mathbf{I} & \dots & -p_{n_p}\mathbf{I}\end{bmatrix}\right)}_{\mathbf{R}} \right)^{-1} \underbrace{\begin{bmatrix}\mathbf{I} & \dots & \mathbf{I}\end{bmatrix}^{\mathrm{T}}}_{\mathbf{E}} s^*\end{aligned} \tag{29}$$

When the matrices $\mathbf{D}$ and $\mathbf{E}^{\mathrm{T}}$ are interchanged, the system is right hand side realized. The order of the resulting system changes from $n_p \cdot n_{outputs}$ to $n_p \cdot n_{inputs}$.

The system can then be cast in the form of an ordinary differential equation (ODE) for the lag states, with $\dot{\mathbf{w}}_j$ as input.

$$\dot{\mathbf{x}}_L = \mathbf{R}\left(\frac{U_\infty}{c_{ref}/2}\right)\mathbf{x}_L + \mathbf{E}\,\dot{\mathbf{w}}_j \tag{30}$$

When using Roger's method, the involved matrices $\mathbf{R}$ and $\mathbf{E}$ have a pronounced sparsity pattern, such that the ODEs are fully decoupled. The order of the system becomes less important from a computational point of view, since no costly matrix multiplications are required for the time integration. The resulting aerodynamic forces are then.

$$\mathbf{P}_g^{aero} = \underbrace{\left(\mathbf{Q^0}_{gj}\,\mathbf{w}_j\right)}_{\text{steady } \mathbf{P}_g^s(\mathbf{w}_j)} + \underbrace{\left(\mathbf{Q^1}_{gj}\left(\frac{c_{ref}/2}{U_\infty}\right)\,\dot{\mathbf{w}}_j + \mathbf{D}\,\mathbf{x}_L(\dot{\mathbf{w}}_j)\right)}_{\text{unsteady } \mathbf{P}_g^u(\dot{\mathbf{w}}_j)} \tag{31}$$

The most significant advantage of the present RFA over the traditional generalized approximation is that equation (31) can be split explicitly into a steady part depending on $\mathbf{w}_j$ and an unsteady part solely depending on $\dot{\mathbf{w}}_j$. The steady part can then be replaced by the present enhanced VLM or even more sophisticated methods. For dynamic manoeuvre simulations the unsteady contribution can be included for fast manoeuvres, or neglected if deemed unnecessary or simulation speed is of concern.

5.3 Unsteady rigid body aerodynamics in nonlinear EoM

In the nonlinear equations of motion (2) the rigid body modes have to be treated differently. The differentiation matrix $\mathbf{D^1}$ relates the orientation $\begin{bmatrix}\varphi & \theta & \psi\end{bmatrix}_b^{\mathrm{T}}$ to a box angle of attack. However, for the nonlinear equations of motion this orientation is defined wrt the geodetic frame of reference and not wrt the freestream. Therefore, the matrix $\mathbf{D^1}_{jk}$ in equation (23) has to be cancelled, i.e. the position and orientation of the aircraft has no influence on the aerodynamics. The angle of attack, respectively sideslip are determined by the velocities $\dot{\mathbf{u}}_b$ wrt a body fixed reference frame. The rationale behind cancelling the $\mathbf{D^1}_{jk}$ term for the nonlinear rigid body motion is equivalent to the absence of the $\mathbf{D^1}_{lk}$ in equation (23). After the transformation $\mathbf{T}_{eb}$ from the center of gravity (index b) to the aerodynamic reference point (index e), the angle of attack α is $\dot{z}_e/U_\infty$ and the sideslip angle β is $\dot{y}_e/U_\infty$, i.e. the normalized heaving and side motion.

$$\mathbf{w}_j(k) = ik \cdot \mathbf{D^2}_{jk}\,\mathbf{\Phi}_{ke}\,\mathbf{T}_{eb}\,\mathbf{u}_b \tag{32}$$

Expressed in the time domain the steady and unsteady contributions are as follows.

$$\mathbf{w}_j = \mathbf{D^2}_{jk}\,\mathbf{\Phi}_{ke}\,\mathbf{T}_{eb}\left(\frac{c_{ref}/2}{U_\infty}\right)\dot{\mathbf{u}}_b \;\;;\;\; \dot{\mathbf{w}}_j = \mathbf{D^2}_{jk}\,\mathbf{\Phi}_{ke}\,\mathbf{T}_{eb}\left(\frac{c_{ref}/2}{U_\infty}\right)\ddot{\mathbf{u}}_b \tag{33}$$

If the aerodynamic matrices are only available in a generalized form, a correction for the rigid body mode shapes has to be applied, when they are used in conjunction with the nonlinear equations of motion. Detailed information on the correction technique can be found in reference [24].

5.4 Gust excitation

Aside from the continuous turbulence, discrete tuned gusts are required [25] for design load calculations. The velocity profile of discrete gust is defined in CS/FAR 25.341 as a gust with a 1-cos shape.

$$v_G = \frac{1}{2} U_0 \left(1 - \cos \frac{2\pi x(t)}{2H}\right) \tag{34}$$

The gust gradient H is the distance parallel to the airplane's flight path from the start of the gust to its peak velocity, Hence the total gust length is $2H$. For a given gust amplitude U_0 several gust gradient distances between $30ft$ and $350ft$ have to be calculated to find the critical response for each load quantity. This process is called gust tuning.

The gust spectrum of a discrete tuned $\mathbf{v}_G(\omega)$ is available semi-analytically for the frequency domain. When the aircraft is subjected to the gust, the penetration speed U_∞ and location of the control points $\mathbf{x}_j$ wrt the gust need to be considered. In the frequency domain these time lags are expressed as phase shifts with an exponential function.

$$\mathbf{w}_j^G(\omega) = \mathbf{n}_j \cdot \exp\left(-i\omega \cdot \mathbf{x}_j / U_\infty\right) \cdot \mathbf{v}_G(\omega)/U_\infty \tag{35}$$

The generalized gust column for the frequency domain can then be set up.

$$\mathbf{Q}_{hG}(k) = \mathbf{\Phi}_{gh}^{\mathrm{T}} \mathbf{Q}_{gj}(k) \mathbf{w}_j^G(\omega) \tag{36}$$

The approximation of this gust column is problematic, due to phase shifts introduced when the aircraft penetrates the gust, cf. eq.(35). This is considered a major problem for application in an large scale industrial context.

An alternative approach is presented that avoids the RFA of the gust column entirely. Examining the physical nature of the gust column reveals that a rational function is not suitable for approximating time shifts Δt. The question arises why an approximation is required in the first place, when the sole purpose is to transfer the gust to the time domain. The downwash at the control points due to a gust $\mathbf{w}_j^G$ (eq. (35)) can simply be expressed as a function of time. The relative location of the airframe wrt the gust is given as.

$$\mathbf{x}_j^G(t) = \mathbf{x}_j + 2H - U_\infty \cdot t \tag{37}$$

The normalized gust velocities are then given as,

$$\mathbf{w}_j^G(t) = \begin{cases} \frac{1}{2U_\infty}\left(1 - \cos\left(\pi \cdot \frac{\mathbf{x}_j^G(t)}{H}\right)\right) \cdot \mathbf{n}_j, & \text{for} \quad 0 < \mathbf{x}_j^G < 2H \\ 0 & \text{otherwise} \end{cases} \tag{38}$$

Differentiation of the normalized gust velocity wrt time yields,

$$\dot{\mathbf{w}}_j^G(t) = \begin{cases} -\frac{\pi}{2H} \cdot \sin\left(\pi \cdot \frac{\mathbf{x}_j^G(t)}{H}\right) \cdot \mathbf{n}_j, & \text{for} \quad 0 < \mathbf{x}_j^G < 2H \\ 0 & \text{otherwise} \end{cases} \tag{39}$$

The approximation of the gust column is avoided completely and the application becomes merely a function evaluation when integrating the ODE. If the velocity of the aircraft is assumed to be constant, the gust is independent of the aircraft simulation and can be pre-computed as a function of Ma, H and U_∞. Subsequently, the results are fed into the overall aircraft simulations.

5.5 Simulation

For the simulation all contributions to the downwash $\mathbf{w}_j(t)$ eq.(40) from rigid body, flexible and control surface motion need to be summed up and connected to the nonlinear equations of motion (2). Unsteady aerodynamics are considered, using the time derivative of the downwash $\dot{\mathbf{w}}_j(t)$ eq. (40) with equations (31) and (30).

$$\mathbf{w}_j = \left\{ \begin{array}{lll} \mathbf{D^2}_{jk}\mathbf{\Phi}_{ke}\mathbf{T}_{eb} & \cdot\left(\frac{c_{ref}/2}{U_\infty}\right) & \dot{\mathbf{u}}_b(t) \\ +\mathbf{D^1}_{jk}\mathbf{\Phi}_{kx} & \cdot & \mathbf{u}_x(t) \\ +\mathbf{D^2}_{jk}\mathbf{\Phi}_{kx} & \cdot\left(\frac{c_{ref}/2}{U_\infty}\right) & \dot{\mathbf{u}}_x(t) \\ +\mathbf{D^1}_{jk}\mathbf{T}_{kg}\mathbf{\Phi}_{gf} & \cdot & \mathbf{u}_f(t) \\ +\mathbf{D^2}_{jk}\mathbf{T}_{kg}\mathbf{\Phi}_{gf} & \cdot\left(\frac{c_{ref}/2}{U_\infty}\right) & \dot{\mathbf{u}}_f(t) \\ +\mathbf{w}_j^G(t) & & \end{array} \right\};\ \dot{\mathbf{w}}_j = \left\{ \begin{array}{lll} \mathbf{D^2}_{jk}\mathbf{\Phi}_{ke}\mathbf{T}_{eb} & \cdot\left(\frac{c_{ref}/2}{U_\infty}\right) & \ddot{\mathbf{u}}_b(t) \\ +\mathbf{D^1}_{jk}\mathbf{\Phi}_{kx} & \cdot & \dot{\mathbf{u}}_x(t) \\ +\mathbf{D^2}_{jk}\mathbf{\Phi}_{kx} & \cdot\left(\frac{c_{ref}/2}{U_\infty}\right) & \ddot{\mathbf{u}}_x(t) \\ +\mathbf{D^1}_{jk}\mathbf{T}_{kg}\mathbf{\Phi}_{gf} & \cdot & \dot{\mathbf{u}}_f(t) \\ +\mathbf{D^2}_{jk}\mathbf{T}_{kg}\mathbf{\Phi}_{gf} & \cdot\left(\frac{c_{ref}/2}{U_\infty}\right) & \ddot{\mathbf{u}}_f(t) \\ +\dot{\mathbf{w}}_j^G(t) & & \end{array} \right\} \tag{40}$$

Further, propulsion and flight control systems are included in the simulation, resulting in an integral nonlinear model for manoeuvre and gust loads analysis, as well as for handling quality investigations.

6 VALIDATION: DISCRETE GUST

To validate the loads analysis model, an open loop discrete gust computation in the time domain with nonlinear equations of motion is compared to a traditional approach using a frequency domain solution. The frequency response is transformed to the time domain using an inverse fast fourier transformation (iFFT) ($\mathcal{F}^{-1}$), cf. [26].

The aim is to compare the effects of using different types of equations of motion, the application of the gust as a function of time, and using time domain integration vs. frequency domain solution. Therefore, the approximated AIC matrices, evaluated at discrete frequencies with eq. (28) are used for the frequency domain solution.

The frequency domain results are obtained by solving the equations of motion (1) for $\mathbf{u}_h(\omega)$. The aerodynamic forces are on the right hand side of eq. (1). Note the dependency on $\mathbf{u}_h$.

$$\mathbf{P}_g^{ext}(\omega) = q_\infty\, \mathbf{T}_{kg}^{\mathrm{T}}\mathbf{S}_{kj}\mathbf{Q}_{jj}(k)\left[\left(\mathbf{D^1}_{jk} + ik\,\mathbf{D^2}_{jk}\right)\mathbf{T}_{kg}\mathbf{\Phi}_{gh}\,\mathbf{u}_h(\omega) + \mathbf{w}_j^G(\omega)\right] \tag{41}$$

The nodal loads can be easily recovered using the mode displacement method in eq. (5) with

$$\mathbf{u}_f(t) = \mathcal{F}^{-1}(\mathbf{u}_f(\omega)) \tag{42}$$

Strongly recommended however is the use of the force summation method in eq. (3), with

$$\mathbf{P}_g^{iner}(t) = \mathcal{F}^{-1}(-\omega^2\mathbf{M}_{gh}\,\mathbf{u}_h(\omega)) \tag{43}$$

and

$$\mathbf{P}_g^{ext}(t) = \mathcal{F}^{-1}(\mathbf{P}_g^{ext}(\omega)). \tag{44}$$

The frequency domain model was evaluated for 1024 frequency points. The obtained loads were superimposed with those from a horizontal flight trim calculation of the nonlinear time domain model.

The model used for the validation is a generic transport aircraft, containing 2040 aerodynamic boxes, 18 control surfaces, and 122 structural grid points. 100 flexible modes were retained. The rational function approximation was done on the basis of splined AIC matrices $\mathbf{Q}_{gj}(k)$, using 12 poles. The aircraft was subjected to a gust with a gust gradient $H = 100ft = 30.48m$ and amplitude $U_0 = 10.16m/s$ the airspeed was $U_\infty = 170.15m/s$ at $Ma = 0.5$ and altitude $h = 0m$. For the time domain simulation the gust was precomputed, using a standard Dormand-Prince `ode45` variable stepsize integrator. The gust forces were fed into an `Simulink` implementation of the presented integral loads analysis model and simulated for $2.5s$.

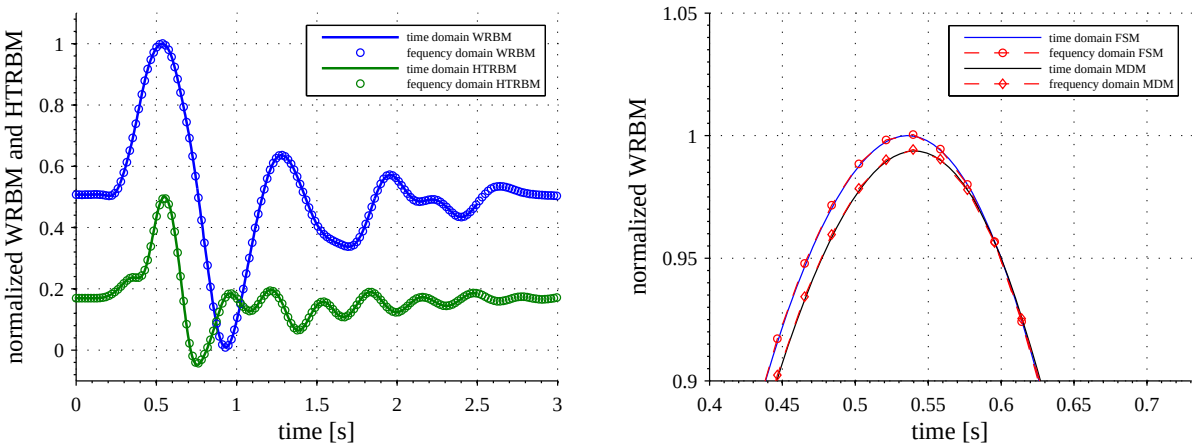

Figure 6: Loads for time and frequency domain solutions

The diagram on the left of figure 6 depicts the integrated wing (WRBM) and horizontal tail root bending moments (HTRBM) for time and frequency domain calculations. The right diagram zooms in on the maximum load for the WRBM and contrasts the MDM with the FSM. The agreement between the time integration and frequency response calculations is excellent. The results are almost indistinguishable.

7 CONCLUSIONS

In this paper an approach for development of integrated models suitable for both gust and manoeuvre loads analysis has been presented. The underlying nonlinear equations of motion, based on a so called "mean axes" system, describe the integrated flight and structural dynamics of the flexible airframe. The data required for the equations of motion is consistent with the classical methods used in loads analysis, i.e the results of a modal analysis of the stiffness and mass data.

For the aerodynamic model a new approach for Rational Function Approximation (RFA) in combination with a suitable selection of boundary conditions has been discussed, allowing for a clear separation between steady and unsteady effects. This allows both effects to be modelled using the most appropriate technique available and for their easy integration.

In this paper, the steady aerodynamic method employed is the commonly used Vortex Lattice Method. The VLM has been enhanced to account for the direction of lifting forces, due to change in relative flow direction, including an induced drag component. This is achieved by using refined boundary conditions, to set up the Kutta-Joukowsky-Law in its

vector cross-product form, as opposed to the commonly used scalar multiplication form. Apart from the induced drag AIC, the required matrices are purely geometric in nature. The aerodynamic

data of the conventional VLM, i.e. $\mathbf{Q}_{jj}(k = 0)$ can be reused. The lift vector with three degrees of freedom of the enhanced VLM induces additional forces and moments at the box reference point. The infinite plate spline matrix was extended to six DoF to accommodate these additional load components.

The unsteady aerodynamics are accounted for by the Doublet Lattice Method. The AIC matrices need to be approximated by an RFA to be available for time domain simulations. Unlike common practice, the RFA is done for the physical AICs rather than their fully generalized form. As already stated, this approach enables a clear separation of steady and unsteady effect and requires the approximation to be carried out only once per Mach number and not for each mass case-Mach number combination. The gust penetration effects are accounted for by simple evaluations for the gust velocities and its time derivative as function of time. This way the problematic approximation of a frequency domain gust column can be avoided entirely.

To connect the steady and unsteady aerodynamics to the nonlinear equations of motion, a special transformation for the rigid body part has to be employed. This is achieved by cancelling the differentiation matrix $\mathbf{D^1}_{jk}$ for the rigid body modes.

As a validation example for the proposed modelling approach, a comparison of a time domain simulation of a discrete gust with the results from a frequency domain calculation has been made. The load quantities were compared in the time domain using an inverse Fourier transformation (iFFT) of the spectra from the frequency domain calculation. The comparison shows excellent agreement of the two different approaches.

Since the present integrated model is simulated in the time domain, it can be used not only for design gusts, but also for investigations involving superposition of gusts and manoeuvres. Furthermore, wind fields dependent on time, position, and aircraft attitude can be examined.

8 APPENDIX: FULLY GENERALIZED VS. PHYSICAL RFA

Responsible for the presence of an acceleration term in the classical RFA, is the additional time derivative in the downwash equation (23). When considering the unsteady contributions $\dot{\mathbf{w}}_j$, the inputs associated with the differentiation matrix $\mathbf{D^2}_{jk}$ is an acceleration, which has to be accounted for in the approximation of the fully generalized AIC matrices. When applying the approximation before multiplication with the differentiation matrices, the acceleration term has to be omitted. Using the latter methodology, it becomes possible to distinguish steady from unsteady contributions.

The classical form of the approximation is obtained from the physical RFA by generalizing the AIC matrices

$$\mathbf{Q}_{hj} = \mathbf{\Phi}_{gh}^{\mathrm{T}}\ \mathbf{T}_{kg}^{\mathrm{T}}\ \mathbf{S}_{kj}\ \mathbf{Q}_{jj} \tag{45}$$

and the two differentiation matrices

$$\mathbf{D^1}_{jh} = \mathbf{D^1}_{jk}\mathbf{T}_{kg}\mathbf{\Phi}_{gh} \ \text{ and } \ \mathbf{D^2}_{jh} = \mathbf{D^2}_{jk}\mathbf{T}_{kg}\mathbf{\Phi}_{gh}. \tag{46}$$

Multiplication and rearrangement of the terms, yields (cf. Roger [20])

$$\tilde{\mathbf{Q}}_{hh}(s^*) = \underbrace{\left(\mathbf{Q^0}_{hj}\mathbf{D^1}_{jh}\right)}_{\tilde{\mathbf{Q}}^{\mathbf{0}}_{hh}} + \underbrace{\left(\mathbf{Q^1}_{hj}\mathbf{D^1}_{jh} + \mathbf{Q^0}_{hj}\mathbf{D^2}_{jh} + \sum_{i=1}^{n_p}\mathbf{Q^{L}}_{i\,hj}\mathbf{D^2}_{jh}\right)}_{\tilde{\mathbf{Q}}^{\mathbf{1}}_{hh}} s^* + \underbrace{\left(\mathbf{Q^1}_{hj}\mathbf{D^2}_{jh}\right)}_{\tilde{\mathbf{Q}}^{\mathbf{2}}_{hh}} s^{*2} + \sum_{i=1}^{n_p}\underbrace{\left(\mathbf{Q^{L}}_{i\,hj}\left(\mathbf{D^1}_{jh} - \mathbf{D^2}_{jh}\, p_i\right)\right)}_{\tilde{\mathbf{Q}}^{\mathbf{L_i}}_{hh}} \frac{s^*\mathbf{I}}{s^* + p_i}. \quad (47)$$

The generalized form in equation (47) however, does not allow to discern between the steady and unsteady contributions anymore. Inspection of equation (40) indicates that the time derivative of the flexible deformation $\dot{\mathbf{u}}_f$ has a quasi-steady part $\mathbf{w}_j$, induced by the heaving motion, as well as an unsteady part $\dot{\mathbf{w}}_j$, due to the change over time. Unfortunately these terms are combined in $\tilde{\mathbf{Q}}^{\mathbf{1}}_{hh}$, making it impossible to use an enhanced steady aerodynamic model from a different source.

9 REFERENCES

[1] Authorities, J. A. *Joint Aviation Regulations - 25, Airworthiness Standards: Transport Category Airplanes*, vol. Subpart C - Structure.

[2] T. Kier, G. Looye, M. Scharpenberg, and M. Reijerkerk (2007). Process, Methods and Tools for Flexible Aircraft Flight Dynamics Model Integration. In *International Forum on Aeroelasticity and Structural Dynamics*, IF-060. CEAS/AIAA.

[3] W.P. Rodden, R.L. Harder, and E.D. Bellinger (1979). Aeroelastic Addition to NASTRAN. Tech. Rep. NASA CR-3094, NASA.

[4] Albano, E. and Rodden, W. (1969). A doublet-lattice method for calculating lift distributions on oscillating surfaces in subsonic flows. *Journal of Aircraft*, 7(2), 279–285.

[5] P. Teufel and M. Kruse (2007). Efficient Method for Coupling Discrete Gust Loads Analysis in the Frequency Domain with a Fully Non-Linear Flight Control System Simulation. In *International Forum on Aeroelasticity and Structural Dynamics*, IF-013. CEAS/AIAA.

[6] M. Karpel, B. Moulin, E. Presente, L. Anguita, C. Maderuelo and H. Climent (2007). Dynamic Response to Gust Excitation with Nonlinear Control Systems. In *International Forum on Aeroelasticity and Structural Dynamics*, IF-072. CEAS/AIAA.

[7] R. J. Guyan (1965). Reduction of stiffness and mass matrices. *Journal of Aircraft*, 3(2), 380.

[8] M. R. Waszak and D. K. Schmidt (1986). On the flight dynamics of aeroelastic vehicles. In *AIAA Atmospheric Flight Mechanics Conference*, AIAA 86-2077. AIAA, pp. 120–133.

[9] M. R. Waszak and D. K. Schmidt (1988). Flight Dynamics of Aeroelastic Vehicles. *Journal of Aircraft*, 25(6), 563–571.

[10] M. R. Waszak, C. S. Buttrill and D. K. Schmidt (1992). Modeling and Model Simplification of Aeroelastic Vehicles: An Overview. Tech. Rep. NASA TM-107691, NASA LARC.

[11] C. Reschke (2006). *Integrated Flight Loads Modelling and Analysis for Flexible Transport Aircraft*. Ph.D. thesis, Universität Stuttgart.

[12] F. Buckens (1963). The Influence of Elastic Components on the Attitude Stability of a Satellite. In *5th Int. Symposium of Space Technology and Science*.

[13] Canavin, J.R. and Likins, P.W. (1977). Floating Reference Frames for Flexible Spacecraft. *Journal of Spacecraft*, 14(12), 724–732.

[14] R. L. Bisplinghoff, H. Ashley, R. L. Halfman (1955). *Aeroelasticity*. Dover Publications Inc.

[15] Hedman, S. (1965). Vortex Lattice Method for Calculation of Quasi Steady State Loadings on Thin Elastic Wings. Tech. Rep. Report 105, Aeronautical Research Institute of Sweden.

[16] Pistolesi, E. (1937). Betrachtungen über die gegenseitige Beeinflussung von Tragflügelsystemen. In *Gesammelte Vorträge der Hauptversammlung 1937 der Lilienthal Gesellschaft*.

[17] J. Katz and A. Plotkin (1991). *Low Speed Aerodynamics: From Wing Theory to Panel Methods*. McGraw-Hill.

[18] W.P. Rodden, J.P. Giesing and T.P. Kalman (1971). New developments and applications of the subsonic doublet-lattice method for nonplanar configurations. In *AGARD Symposium on unsteady aerodynamics for aeroelastic analyses of interfering surfaces*, AGARD-CP-80-71. AGARD.

[19] R.L. Harder and R.N. Desmarais (1972). Interpolation Using Surface Splines. *Journal of Aircraft*, 9(2), 189–191.

[20] Roger, K. L. (1977). Airplane math modeling methods for active control design. In *AGARD Structures and Materials Panel*, AGARD/CP-228. AGARD, pp. 4–1 – 4–11.

[21] R. Vepa (1977). Finite State Modeling of Aeroelastic Systems. Tech. Rep. NASA CR-2779, NASA.

[22] I. Abel (1979). An analytical technique for predicting the characteristics of a flexible wing equipped with an active flutter-suppression system and comparison with wind-tunnel data. Tech. Rep. NASA TP-1367, NASA LARC.

[23] M. Karpel (1981). Design for Active and Passive Flutter Suppression and Gust Alleviation. Tech. Rep. NASA CR-3482, NASA.

[24] Looye, G. (2005). Integration of rigid and aeroelastic aircraft models using the residualised model method. In *International Forum on Aeroelasticity and Structural Dynamics*, IF-046. CEAS/DLR/AIAA.

[25] Hoblit, F. M. (1988). *Gust Loads on Aircraft: Concepts and Applications*. AIAA Education Series.

[26] M. Karpel, V. Feldgun and B. Moulin (2007). Dynamic Response of Aeroelastic Systems Using Fast Fourier Transforms. In *International Forum on Aeroelasticity and Structural Dynamics*, IF-049. CEAS/AIAA.